



# A novel toolpath for 7-NC grinding of blades with force-position matching

Yilin Mu<sup>1</sup> · Chong Lv<sup>1</sup> · Heng Li<sup>1</sup> · Lai Zou<sup>1</sup> · Wenxi Wang<sup>1</sup> · Yun Huang<sup>1</sup>

Received: 19 April 2022 / Accepted: 10 September 2022 / Published online: 28 September 2022  
© The Author(s), under exclusive licence to Springer-Verlag London Ltd., part of Springer Nature 2022

## Abstract

The characteristic of uneven machining allowance of blades and the flexible contact properties of the belt grinding makes the traditional toolpath of the grinding tool difficult to precisely control the machining profile. In this paper, a novel toolpath planning method based on force-position matching is proposed to perform an efficient grinding process for aero-engine blades. A material removal rate (MRR) model is established through the orthogonal grinding experiments of titanium alloy sample, and the point-by-point adjustment of the 7th axis is controlled based on this model and the machining allowance distribution. Subsequently, the step length is calculated based on the Taylor expansion method, and the post-processing generation of the self-developed 7th axis NC machining tool is carried out based on the double vector control method. On this basis, the comparative experimental results revealed that the average surface profile accuracy of blades of the proposed method was 0.019 mm, which was improved by 54.76% than that of the traditional method. Moreover, the average surface roughness and the variation range of surface roughness were achieved to 0.34  $\mu\text{m}$  and 0.14  $\mu\text{m}$ , which were improved by 27.7% and 33.3% than that of the former method. It is concluded that this research is beneficial to comprehensively improve the machined quality of blades with uneven machining allowance distribution in NC belt grinding.

**Keywords** NC grinding · Aero-engine blade · Uneven allowance distribution · Force-position matching · Toolpath

## 1 Introduction

As the core part of aero-engines, the machining accuracy of blades directly determines the service performance and working life of the aero-engine [1]. The blade after finish milling has obvious cutting lines and uneven machining allowance distribution, which requires further grinding and polishing [2, 3]. The traditional toolpath planning method of NC belt grinding machine tool only considers the geometric interpolation of the machined surface, while the MRR and the uneven machining allowance distribution are ignored. Therefore, it has to divide the desired machining region into multiple patches and perform multiple grinding in each patch to ensure the machining accuracy. This process is time-consuming and laborious, which relies heavily on manual experience. It is well known that the MRR model, toolpath planning method, and the grinding tool axis vector control are the key basis to keep the machining accuracy in the NC abrasive belt grinding process.

Many researchers have done a lot of research on MRR model. Wu et al. [4] proposed a shape-dependent model to estimate the material removal of grinding geometrically complex workpieces, which introduced local coefficients to represent the material removal ability of the system under some contact conditions. Wei et al. [5] proposed a new abrasive flow machining material removal prediction model, which could accurately predict the change of profile height of materials  $\Delta H$  and quality change trend  $\Delta M$ . The prediction error of the validation experiment was 6.4% and 6.9%, respectively. Qi et al. [6] proposed a prediction model of the material removal depth, which fully took into account the impact of the abrasive grains characteristics on the depth of removal. Ren et al. [7] established a MRR model based on Preston equation, which studied the influence of polishing parameters on the deviation characteristics of material removal profile by single factor analysis and Taguchi method. Yang et al. [8] established a new MRR model based on the motion trajectory of a single spherical abrasive particle, which could significantly reduce the root mean square error, as well as mean absolute percentage error values, from 18.426 to 14.942%, respectively. Wang et al. [9] established a MRR model to predict the material removal depth on

✉ Chong Lv  
lvzongchong@163.com

<sup>1</sup> State Key Laboratory of Mechanical Transmissions,  
Chongqing University, Chongqing 400044, China

the workpiece surface, which considered the influence of abrasive particle size on material removal depth. Li et al. [10] proposed a theoretical model of local and overall material removal according to the sliding trajectory of abrasive particles and chemical mechanical synergy, and analyzed the distribution of material removal on wafer surface. Fan et al. [11] proposed a new method to model and optimize material removal during polishing, which focused on the effect of the sliding velocity on the material removal profile. Fan et al. [12] established a numerical model of material removal quantity from a microscopic point of view, taking into account the characteristics of abrasive particles and their interactions. Satyarthi and Pandey [13] established the MRR model in electric discharge grinding. The percentage difference between the experimental results and the theoretical prediction was less than 3%. Kumar and Dvivedi [14] developed a predictive model of MRR for a novel ultrasonic turning process, which adopted Taguchi grey relational analysis to optimize process parameters. Zarepour and Yeo [15] presented a model to predict ductile and brittle material removal modes when a brittle material is impacted by a single sharp abrasive particle in micro ultrasonic machining process. Bhavsar et al. [16] conducted the focused ion beam micro-milling experiment on cemented carbide according to the L16 orthogonal array of Taguchi technique, and used the Pareto optimal solution generated by genetic algorithm to represent the optimal value of MRR in multi-objective optimization. The above MRR model analyzed the impact of different process parameters on the material removal rate, and combined with the interaction of particles at the micro level. However, only considering the material removal model cannot solve the machining problem of the aero-engine blade with large curvature changes.

In addition, Fan et al. [17] proposed an interpolation scheme using cubic Bezier curve to solve the problem that the tool path generated by G01 in CAM system was not smooth. Sarkar and Dey [18] proposed a new iso-parametric toolpath planning for machining trimmed freeform surfaces. In this method, the partial differential equation method and the newly developed boundary interpolation method were used to re-parameterize the trimmed surface. Hu et al. [19] proposed a planar tool path generation algorithm for multi axis machining of free-form surface, which fully considered the width of cutting belt and the movement ability of machine. Huang et al. [20] proposed a trajectory planning method based on machining accuracy control, and to avoid local interference, the radius of the contact wheel should be less than the minimum radius of curvature of the grinding point. Ma et al. [21] further refined the key contact points, and generated the target points of surface curvature mutation or surface intersection in the sensitive area of the workpiece, basing on the curvature change rate and curve length criteria. Wen et al. [22] proposed that the interval spacing

between neighboring path segments was determined by the contact area, which was position-dependent and varied along the surface in accordance with its principal curvatures. Li et al. [23] used dual-cubic NURBS curves to determine the path points and axis vectors on a detection path, and finally obtained a smooth and interference free detection path. Wang et al. [24] used tangent point method and coordinate transformation theory to generate tool feed path when the surface morphology of tool and workpiece could be described by mathematical method. Zhao et al. [25] proposed a dual quaternion B-spline approximation method of dominant points to generate smooth tool paths for five-axis CNC machine tools. Sun and Altintas [26] presented a geometric smoothing algorithm by enforcing the continuity of first, second, and third geometric derivatives of the splined path segments at their meeting points for the five-axis machining of curved surfaces. Yang et al. [27] proposed a tool path generation algorithm, in which the tool tip position was represented by a third-order B-spline curve and the tool direction was represented by a third-order polynomial spline curve to obtain a continuous tool path. Chaves-Jacobs et al. [28] used quintic polynomial interpolation to generate optimized tool paths for five axis machine tools and industrial robots, thereby improving tool wear and surface coverage during polishing. Hatem et al. [29] developed an algorithm for calculating the finish machining tool path based on the two-dimensional curve offset and polygon chain intersection algorithm, which solved the time-consuming calculation involved in calculating the cutter location surface of the measured data. Tajima and Sencer [30] proposed a new real-time interpolation algorithm for NC systems to generate continuous rapid feed motion along short segmented linear tool-paths by smoothing local and adjacent corners that were within close vicinity. Most of the above toolpath generated method considered the change of curvature when generating the toolpath, but due to the complexity of MRR model and the uneven distribution of machining allowance, the toolpath generated by these method is hard to machine the blade within the tolerance range in the NC grinding.

The main difficulties in NC belt grinding are the accurate MRR model and reliable toolpath planning method. However, these factors are only considered separately in the above methods, which is difficult to ensure the machining accuracy of blades due to the lack of control of the grinding process parameters. Therefore, we independently developed the 7th axis NC abrasive belt grinding machine tool, in order to more conveniently control the processing parameters. This equipment features high path precision and favorable adaptation. Besides, the elastic grinding wheel features good elasticity as well as rapid cooling under high-speed revolution, so the equipment is applicable to grind the complex curved part. Consequently, a novel toolpath planning method is proposed for aero-engine blades with the uneven machining

allowance distribution to realize the point-by-point adjustment. The orthogonal tests were used to obtain the relationship between the pressing amount of the 7th axis (*U* axis) and the material removal depth. Finally, the variable pressing amount grinding experiments were carried out to verify the feasibility of the proposed method.

## 2 MRR model

### 2.1 Force-position matching

The force-position matching unit of the 7-axis NC machine tool (*X/Y/Z/A/B/C/U*) shown in Fig. 1a is mainly composed of servo motor, synchronous belt, nut pulley, screw rod, spring damper, guide rod and contact wheel. The *U* axis in the floating grinding mechanism is fixed on the *C* axis as the 7th axis and moves along the *Z* axis to realize micro flexible grinding. The working principle of the force-position matching unit is shown in Fig. 1b, the servo motor drives the synchronous belt to rotate, and then drives the screw rod to move up and down, so as to make the spring damper at the end of the screw rod, the guide rod and the contact wheel move slightly. The grinding tool keeps a floating contact with the workpiece due to the spring damper. When the contact wheel contacts the workpiece, the gravity of the guide rod and the contact wheel is balanced with the spring force to maintain the required grinding normal pressure. And when the normal pressure needs to be increased, the servo motor drives the guide rod and the contact wheel to move downward to reduce the spring force. Similarly, the normal grinding pressure can be reduced by reversing the servo motor. Point-by-point adjustment of force-position matching can be achieved by adjusting the pressing amount of the *U*-axis at each machining point.

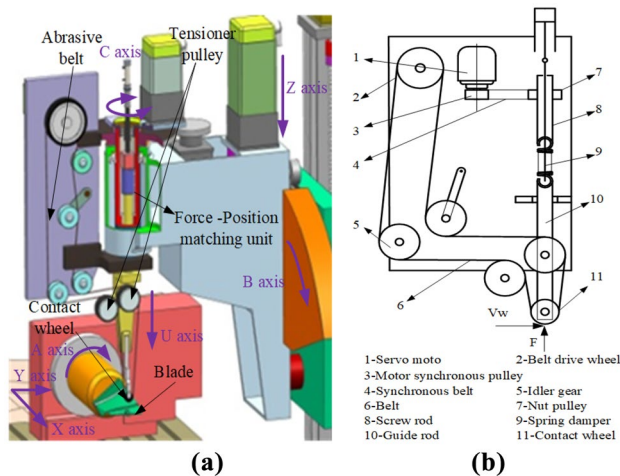


Fig. 1 Seven-axis linkage NC belt grinder. a Force-position matching unit. b Working principle diagram of force-position matching unit

The material removal depth  $a_p$  of the workpiece during the abrasive belt grinding process is mainly related to the processing parameters such as the workpiece feedrate  $v_w$ , belt linear speed  $v_s$ , normal contact pressure  $F$  and so on. That is

$$a_p = f(v_s, v_w, F) \tag{1}$$

In the floating grinding mechanism, the pressing amount  $U$  of *U*-axis is not the actual material removal depth due to the existence of spring damper. Besides, the normal contact pressure between the contact wheel and the blade causes the elastic deformation of the rubber contact wheel. Therefore, the relationship between the normal contact pressure and the pressing amount is nonlinear. The functional relationship of the set pressing amount  $U$  and the normal contact force  $F$  is expressed as below.

$$F = g(U) \tag{2}$$

In the actual grinding process, it is difficult to directly control the normal contact force  $F$  at each machining point to a desired value because of the system response time and system construction cost. However, the normal contact pressure can be adjusted by indirectly controlling the pressing amount  $U$  point-by-point to realize the accurate material removal. Therefore, the material removal depth is established by the following formula.

$$a_p = f(v_s, v_w, U) \tag{3}$$

### 2.2 Nonlinear regression prediction model

In order to quantitatively determine the nonlinear relationship between the pressing amount  $U$  and the material removal depth  $a_p$ , the material removal model is established through the orthogonal grinding experiment of titanium alloy samples. Based on the previous research of our group [1], the main process parameters of the orthogonal grinding experiment with 3 factors and 4 levels are shown in Table 1. Figure 2a shows the NC abrasive belt grinding process of the titanium alloy sample. Due to the rubber material of the contact wheel, elastic deformation occurs when the contact wheel contacts the workpiece, which is photographed by high-speed camera Revealer 5KF20. And it can be found that the deformation degree of the grinding tool is not only related to the rubber material, but also has a great relationship with the grinding speed of the grinding tool during the experiment.

The retec MFT-5000 white light interferometer is used to measure the material removal depth, and the results are shown in Table 2. It can be seen that the relationship between the pressing amount  $U$  and the material removal

**Table 1** Main processing parameters of orthogonal grinding tests

Main parameters	Values
Grinding speed $v_s$ (m/s)	6.28,7.85,9.42,11.00
Feed rate $v_w$ (mm/s)	14,17,20,24
Pressing amount $U$ (mm)	3,5,7,9
Contact wheel radius $R$ (mm)	15
Contact wheel width $W_a$ (mm)	5
Lubrication condition	Dry grinding

depth  $a_p$  is nonlinear. Besides, the pressing amount  $U$  and the material removal depth  $a_p$  are not on the same order of magnitude. With the linear change of  $U$ , the rubber wheel deforms to varying degrees, and the material removal depth  $a_p$  can not change linearly. Figure 2b shows the grinding profile under the No.12 experimental parameters, which indicates the contact pressure is the largest in the contact center and decreases along the diameter direction.

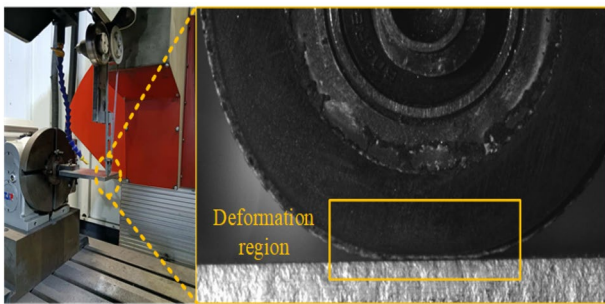
According to the results shown in Table 2, the relationship between the material removal depth  $a_p$  and grinding process parameters (abrasive belt linear speed  $v_s$ , workpiece feedrate  $v_w$ , pressing amount  $U$ ) is obtained by the multiple linear regression method. By minimizing the residual of the regression model, the parameters in the formula are calculated by the least square method.

**Table 2** Results of the orthogonal experiment

No	$v_s$ (m/s)	$v_w$ (mm/s)	$U$ (mm)	$a_p$ ( $\mu\text{m}$ )
1	6.28	14	3	3.63
2	6.28	17	5	3.53
3	6.28	20	7	3.22
4	6.28	24	9	3.78
5	7.85	14	5	4.70
6	7.85	17	3	4.32
7	7.85	20	9	4.44
8	7.85	24	7	4.23
9	9.42	14	7	5.14
10	9.42	17	9	5.64
11	9.42	20	3	5.24
12	9.42	24	5	5.53
13	11.00	14	9	9.28
14	11.00	17	7	5.85
15	11.00	20	5	5.65
16	11.00	24	3	5.18

$$a_p = 0.933v_s^{1.039}v_w^{-0.269}U^{0.119} \tag{4}$$

The result of multiple linear regression shows that the goodness of fit  $R^2$  and correction measurement coefficient  $R^2_{adj}$  of the regression equation are 85 and 81%, respectively, which are greater than 80%, indicating that the regression equation has a good fitting effect and can reflect the actual measured data. The critical value at the significance level  $F_\alpha$  is  $3.07 \times 10^{-5}$ , which is less than 0.02%. Thus, the confidence of the regression equation can reach more than 99.98%, which indicates that the above equation can accurately reflect the relationship between the material removal depth and the grinding process parameters.



### 3 Toolpath planning

#### 3.1 Step length calculation

The step length is the distance between two adjacent cutter-contact (CC) points, which directly affects the machining accuracy. Taking the  $u$ -direction grinding as an example, the current toolpath  $P(u)$  shown in Fig. 3 can be expressed as in the parameter domain

$$P(u) = (x(u), y(u), z(u)) \tag{5}$$

where,  $x(u)$ ,  $y(u)$ ,  $z(u)$  represent the coordinates of CC point in the spatial coordinate system.

The variable  $u$  can be regarded as a function of time  $t$ , then perform a Taylor expansion of the parameter  $u$  at  $t = t_i$ ,

**Fig. 2** Photograph of orthogonal grinding experiments. **a** Elastic deformation of rubber wheel. **b** Profile of grinding area

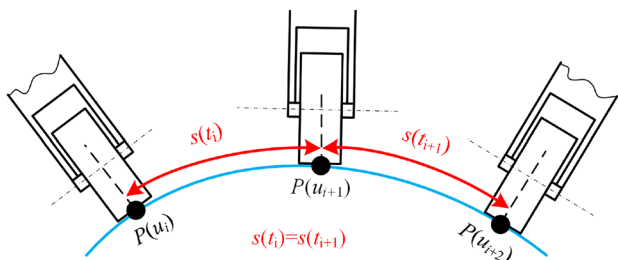


Fig. 3 Schematic diagram of step-length calculation

$$u(t) = u(t_i) + \frac{du}{dt} \Big|_{t=t_i} (t - t_i) + \frac{d^2u}{dt^2} \Big|_{t=t_i} \frac{(t - t_i)^2}{2!} + \dots + \frac{d^n u}{dt^n} \Big|_{t=t_i} \frac{(t - t_i)^n}{n!} \tag{6}$$

Let  $u_i = u(t_i)$ , then there is

$$u_{i+1} = u_i + T \frac{du}{dt} \Big|_{t=t_i} + \frac{T^2}{2} \frac{d^2u}{dt^2} \Big|_{t=t_i} + HOT \tag{7}$$

where,  $T$  is the interpolation cycle, and  $HOT$  is the high-order infinitesimals.

The interpolation cycle  $T$  of the machine tool is generally very short, and the high-order term is almost equal to zero, which can be ignored.

$$u_{i+1} \approx u_i + T \frac{du}{dt} \Big|_{t=t_i} + \frac{T^2}{2} \frac{d^2u}{dt^2} \Big|_{t=t_i} \tag{8}$$

Let the interpolation speed of the toolpath be  $v(u_i)$ , then

$$\begin{cases} v(u_i) = \left| \frac{dP(u)}{dt} \right|_{u=u_i} = \left| \frac{dP(u)}{du} \right|_{u=u_i} \cdot \frac{du}{dt} \Big|_{t=t_i} \\ \frac{du}{dt} \Big|_{t=t_i} = \frac{v(u_i)}{\left| \frac{dP(u)}{du} \right|_{u=u_i}} \end{cases} \tag{9}$$

Taking the derivative on both sides of the first derivative equation of the above formula, and get the second derivative shown in the following equation.

$$\frac{d^2u}{dt^2} \Big|_{t=t_i} = - \frac{v^2(u_i) \left( \frac{dP(u)}{du} \cdot \frac{d^2P(u)}{du^2} \right)}{\left| \frac{dP(u)}{du} \right|_{u=u_i}^4} \tag{10}$$

The toolpath interpolation formula of the second-order Taylor expansion can be obtained by

$$u_{i+1} = u_i + \frac{s}{\sqrt{x_i'^2 + y_i'^2 + z_i'^2}} - \frac{s^2}{2} \frac{(x_i''x_i'' + y_i''y_i'' + z_i''z_i'')}{(x_i'^2 + y_i'^2 + z_i'^2)^2} \tag{11}$$

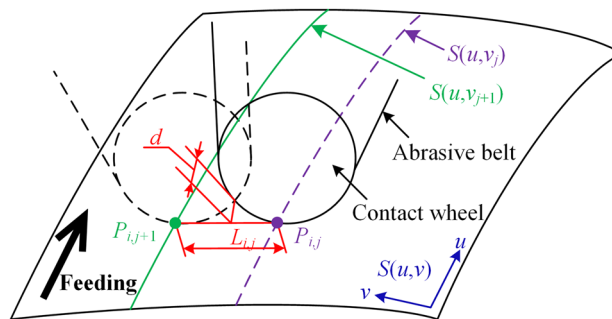


Fig. 4 Schematic diagram of row spacing calculation

Where,  $(x_i', y_i', z_i')$  and  $(x_i'', y_i'', z_i'')$  are the first and second derivative of the current CC point respectively,  $s$  is the step length. The traditional step length determination methods include iso-parametric method and constant chord error method [31], which can generate dense CC points at the positions with large curvature changes and sparse CC points at the positions of small curvature changes. However, due to the surface contact state and the small size of the edge, over-grinding is easy to occur in the places with dense CC points, resulting in the scrap of the machining blades. Therefore, this paper proposes the equal arc length discretization to discretize the machining path equably, keeping the distance consistent between the adjacent CC points in cartesian space. Then, the next CC point  $P(u_{i+1})$  of the current toolpath can be calculated according to the current point  $P(u_i)$  and the set step length  $s$ .

### 3.2 Toolpath interval

The iso-scallop method is used to generate the next toolpath, which fully considers the curvature changes of the complex surface, the tool radius and the machining accuracy. The toolpath interval  $L_{i,j}$  shown in Fig. 4 between the CC point  $P_{i,j}$  and the CC point  $P_{i,j+1}$  can be calculated through the local geometric contact information. Taking the  $u$ -direction grinding as an example, the minimum value of  $v$  ( $v_{min}$ ) parameter is taken as the the parameter of the next toolpath, so as to avoid the severe processing vibration caused by the uneven distribution of CC points or self-intersection. A detailed description of the toolpath interval calculation can be found in the literature [32]. Figure 5 schematically shows two toolpath generation methods for the NC grinding of complex blade. The proposed method controls the pressing amount of  $U$ -axis point-by-point according to the machining allowance of each CC point and MRR model, realizing the application of MRR model in toolpath planning through the NC machining program generated by our self-developed CAM software.

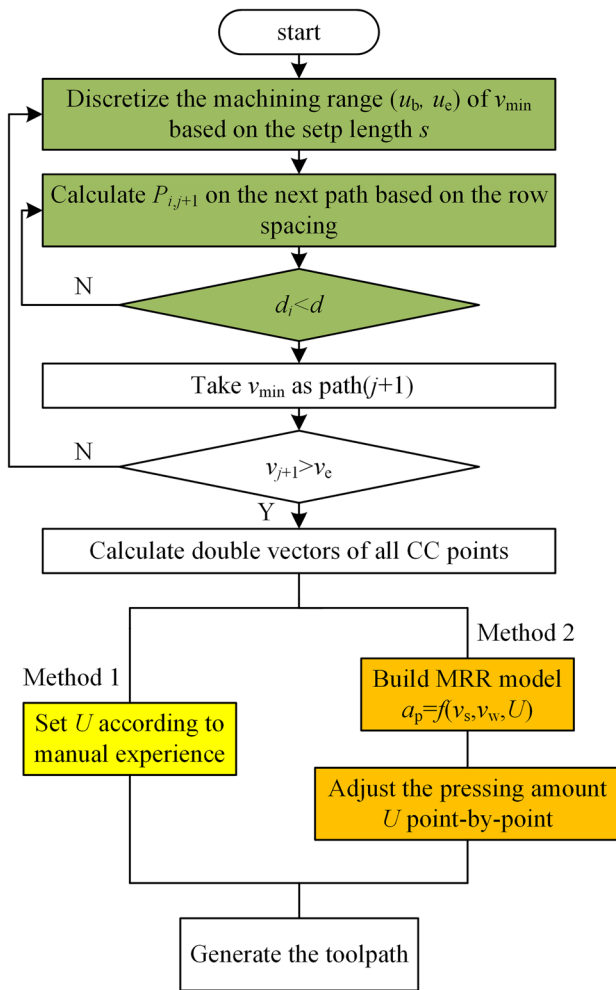


Fig. 5 Flowchart of two toolpath generation methods

### 4 Post-processing algorithm of CC points

Unlike the 5-axis milling, which controls only one direction of the cutting tool, NC abrasive belt grinding needs to control the two directions of the grinding tool (the support axis direction and the axis direction). In order to keep a best contact state between the grinding tool and the blade, this paper ensures that the support axis of the grinding tool is in the same direction with the normal vector of CC points through the rotation of axis A and B, and the axis direction is in the same direction with the tangent direction of CC points through the rotation of axis C. This control method of tool directions can not only control the normal contact pressure conveniently, but also avoid the severe vibration caused by the excessive swing of the grinding tool.

Taking the workpiece as the object, the workpiece coordinate system  $O_p X_p Y_p Z_p$  is established, which maintains the same attitude as the machine tool coordinate system

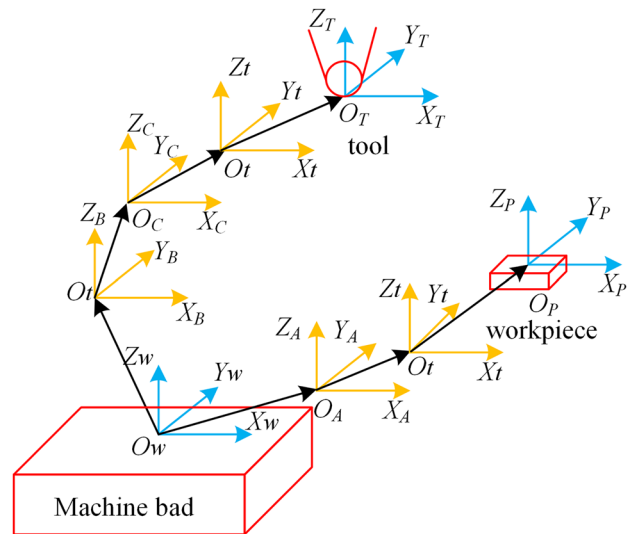


Fig. 6 Establishment of machine tool coordinate system

$O_w X_w Y_w Z_w$ , as shown in Fig. 6. In order to make the support axis direction of the contact wheel follow the normal direction of the CC point, firstly rotate the normal vector  $n_0 = [n_{x0}, n_{y0}, n_{z0}]^T$  of the CC point around the X axis to the XOZ plane, and ensure the rotation angle is  $[-180^\circ, 180^\circ]$ , which is recorded as angle A.

$$A = \begin{cases} \arctan\left(\frac{n_{y0}}{n_{z0}}\right) (n_{z0} > 0) \\ \pi + \arctan\left(\frac{n_{y0}}{n_{z0}}\right) (n_{z0} < 0) \\ \frac{\pi}{2} (n_{y0} > 0, n_{z0} = 0) \\ -\frac{\pi}{2} (n_{y0} < 0, n_{z0} = 0) \end{cases} \quad (12)$$

In order to solve the angle B, it is necessary to know the attitude of the normal vector after rotating angle A around, which is expressed as  $n_1 = [n_{x1}, n_{y1}, n_{z1}]^T$ . Then the value of angle B shown in Fig. 7 is expressed by

$$B = -\arctan\left(\frac{n_{x1}}{n_{z1}}\right) = -\arctan\left(\frac{n_{x0}}{\sqrt{(n_{y0})^2 + (n_{z0})^2}}\right) \quad (13)$$

Set the initial axis direction of the grinding tool in  $O_w X_w Y_w Z_w$  to  $[1, 0, 0]^T$ , the initial tangent direction  $[\tau_x, \tau_y, \tau_z]^T$  of each CC point can be solved based on the relevant knowledge of differential geometry. In order to keep the axis direction in the same direction as the tangent direction at each CC point, the tangent direction must be rotated by a C angle around the

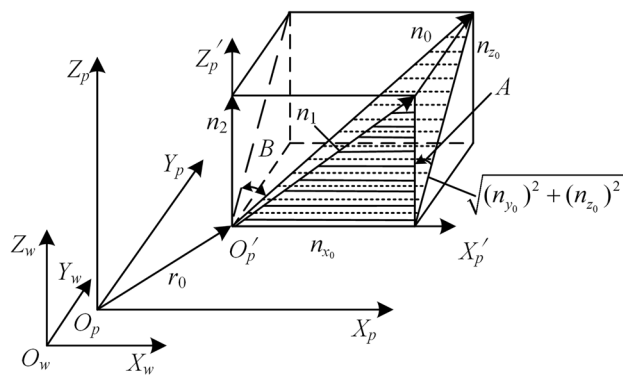


Fig. 7 Calculation of angle A and B

Z axis of the rotation center of the C axis after the coordinate transformation. At this time, the new tangent direction  $[\tau'_x, \tau'_y, \tau'_z]^T$  becomes

$$\begin{bmatrix} \tau'_x \\ \tau'_y \\ \tau'_z \end{bmatrix} = Rot(y, B) \times Rot(x, A) \times \begin{bmatrix} \tau_x \\ \tau_y \\ \tau_z \end{bmatrix} \tag{14}$$

Thus

$$C = \arctan\left(\frac{\tau'_y}{\tau'_z}\right) \tag{15}$$

Due to the movement of axis A and axis B, the position of each point  $[x_0, y_0, z_0]^T$  in the workpiece coordinate system will also change accordingly. Firstly, the coordinate value of each point is solved. Then, the coordinate relationship

$[x_h, y_h, z_h]^T$  between the workpiece coordinate system and the machine tool coordinate system is established. After the coordinate transformation, the coordinate value of the CC point in the machine tool coordinate system is solved, which is expressed as  $[x, y, z]^T$ , therefore

$$\begin{bmatrix} x \\ y \\ z \end{bmatrix} = Trans(x_h, y_h, z_h) \times Rot(y, B) \times Rot(x, A) \times \begin{bmatrix} x_0 \\ y_0 \\ z_0 \end{bmatrix} \tag{16}$$

Then

$$\begin{cases} x = x_0 \cos B + y_0 \sin A \sin B + z_0 \cos A \sin B + x_h \\ y = y_0 \cos A - z_0 \sin A + y_h \\ z = -x_0 \sin B + y_0 \sin A \cos B + z_0 \cos A \cos B + z_h \end{cases} \tag{17}$$

## 5 Comparative grinding experiments

### 5.1 Experimental setup

Figure 8b shows the self-developed 7-axis NC abrasive belt grinding machine tool specially used for grinding various blades. The blade is clamped on the turntable (A axis) through the fixture, and the turntable is located on the workbench composed of the X axis and Y axis. The force-position matching unit can move up and down along the Z axis and rotate around the Y axis (B axis). In addition, the 7th axis can rotate slightly around the grinding axis direction (C axis) and move up and down slightly along the support axis direction

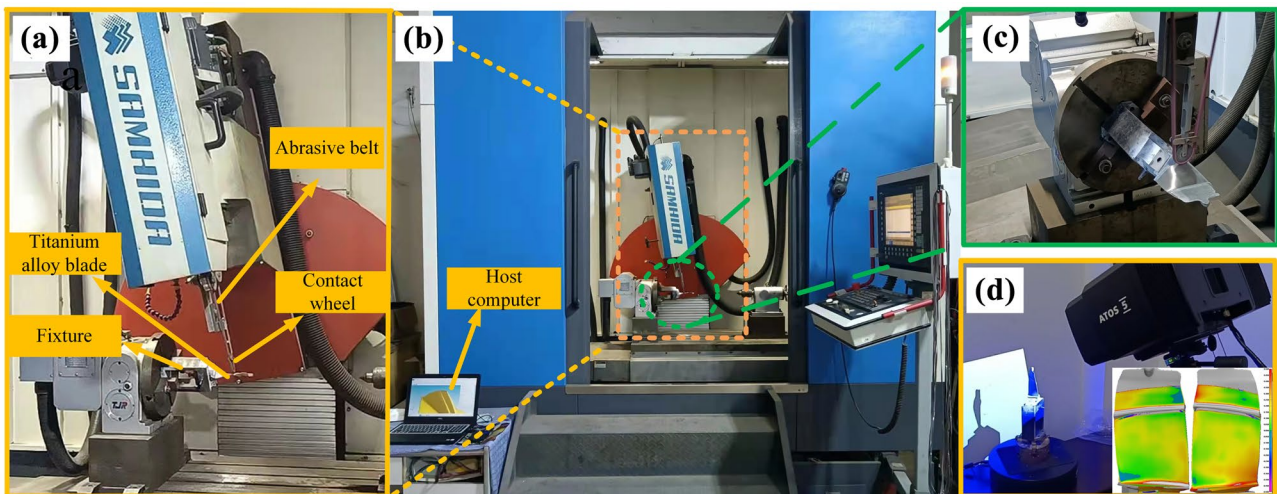
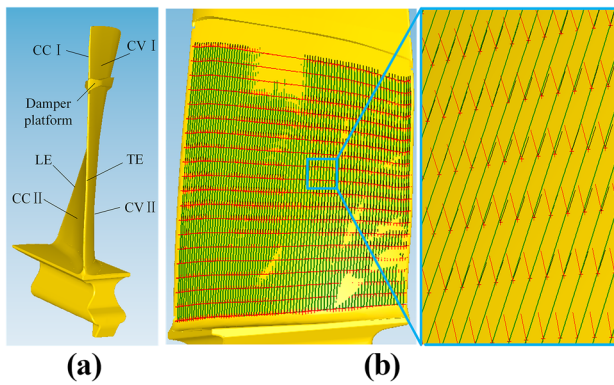


Fig. 8 Experimental setup. a Force-position matching unit. b NC grinding platform. c Grinding process. d GOM Blue-ray scanning device



**Fig. 9** Toolpath generation. **a** Region division. **b** Toolpath of CV II

of the grinding tool. Figure 8a shows the Ti-6Al-4 V alloy blade with the dimension of 140 mm × 60 mm × 25 mm fixed at the end of the fixture. Figure 8c shows the actual grinding process of the blade, in which the contact wheel is mainly composed of aluminum as the core material and elastic rubber (15–20 HRC) as the outer layer. The GOM ATOS 5 Airfoil Blu-ray scanning device is used to quickly obtain the actual model of the blade, and the machining allowance deviation is shown in Fig. 8d.

According to the structural characteristics of the blade shown in Fig. 9a, the processing region of the blade is divided into four areas: CC, CV, LE and TE. In addition, the CC/CV part is divided into I and II parts due to the damper platform. The damper platform of the blade is not considered to be machined with these methods to reduce the time of grinding experiments. Referring to the previous relevant research work [1], the pyramid A6 abrasive belt (P2000) is used to grind the LE and TE as the advantages of continuous self-sharpening and grinding consistency, and the red nylon belt is used for polishing the CC and CV to improve surface roughness. The specific grinding scheme is shown in Table 3. Figure 9b shows the machining toolpath generated in the independently developed CAM software, in which the red line represents the support axis direction of the grinding tool, the black line represents the axis direction of the grinding tool, and the green curve represents the machining toolpath.

**Table 3** Main processing parameters of comparative experiments

Main parameters	Traditional toolpath		Proposed toolpath		
	Processing area	CC,CV	LE,TE	CC,CV	LE,TE
Belt type	Red nylon belt	3 M pyramid belt A6	Red nylon belt	3 M pyramid belt A6	
$v_s$ (m/s)	7.85				
$v_w$ (mm/min)	1000				
$u$ (mm)	20				The proposed method
Contact wheel	Φ30×5				

## 5.2 Discussion

### 5.2.1 Surface roughness

The machined surface roughness of the blade was measured along the direction perpendicular to the grinding speed by the Taylor Hobson FTS intra type roughness meter, as shown in Fig. 10a. Each region of the blade was sampled five times, and the average surface roughness was calculated to reduce the measurement error. It can be seen from Fig. 10b that the average surface roughness of the blade machined by the traditional toolpath method was 0.47  $\mu\text{m}$ , and the surface roughness of the proposed toolpath method was 0.34  $\mu\text{m}$ , which was improved by 27.7%. And the variation range of surface roughness in different areas of the proposed toolpath planning method is greatly improved compared with the traditional one. Besides, the variation range of surface roughness of the blade machined by the traditional toolpath method was 0.21  $\mu\text{m}$ , and the variation range of surface roughness of the proposed toolpath method was 0.14  $\mu\text{m}$ , which was improved by 33.3% than the traditional method. This is because the proposed MRR model can achieve a precise.

material removal at each CC point, making the machined surface smoother and closer to the theoretical surface, which can improve the consistency of surface roughness. However, the material removal rate of all CC points in the traditional method are all consistent. That is, the machined surface profile is similar to the blade blank, and the machining allowance is still uneven.

### 5.2.2 Machine efficiency

Figure 11 shows the machining efficiency comparison at each machining region by using two toolpath methods. It can be seen that the machining efficiency of the two methods is basically the same. This is because the processing point information on these two kinds of toolpath is consistent. Although the second processing method introduces the 7th axis, its control response time is consistent with the other six axes due to the high response of NC machine tool. It should be noted that the proposed method needs to calculate the MRR model and pressing amount of each CC point, the toolpath calculation time is slightly higher than that of the traditional one, but within an acceptable range.



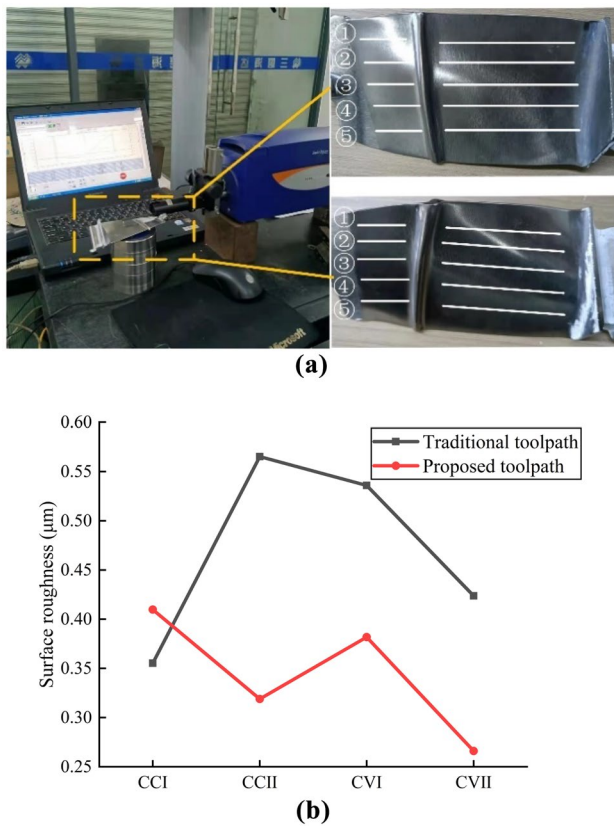


Fig. 10 Surface roughness measurement. a Measurement process. b Measurement results

### 5.2.3 Profile accuracy

The profile accuracy of blades was measured using the Hexagon global series three coordinate-measuring machines. The measuring results of six sections of each blade were

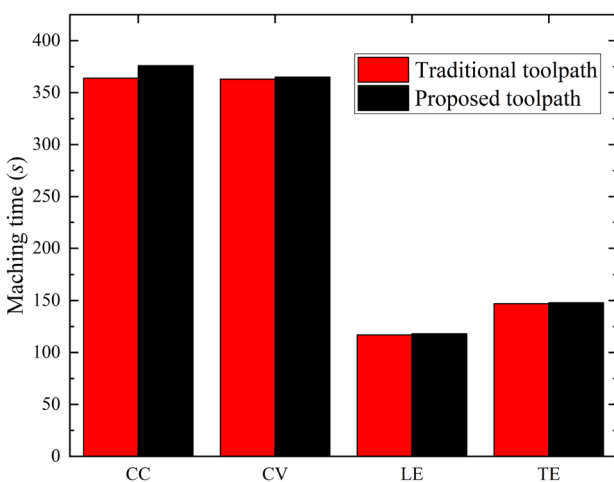
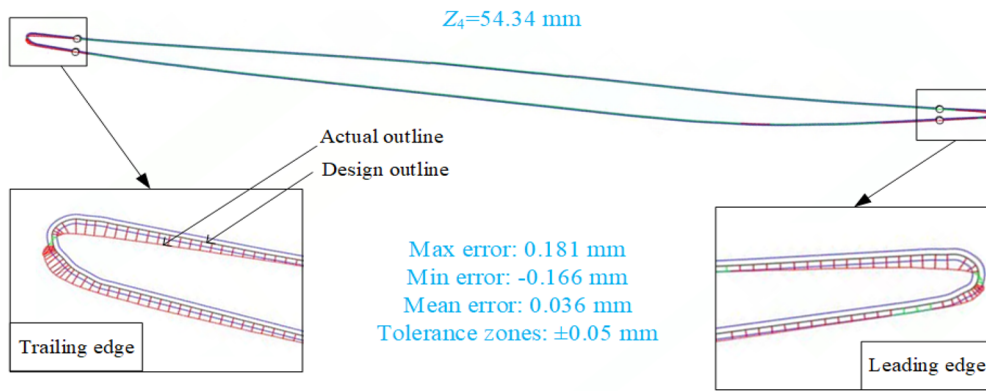


Fig. 11 Machining time of each region

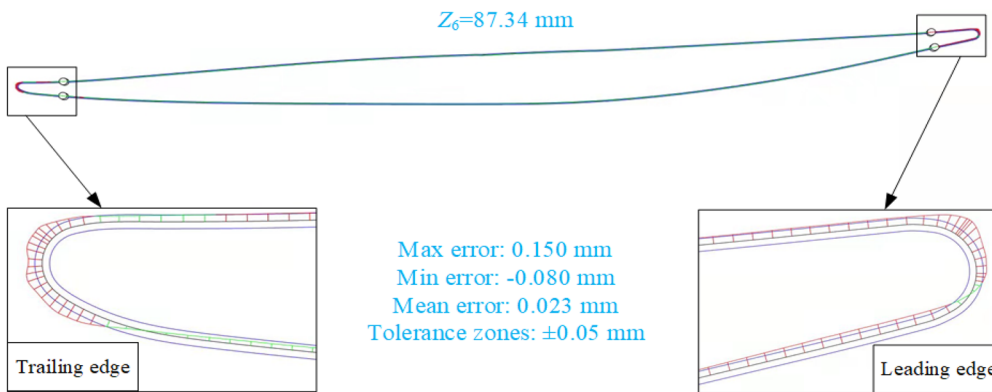
measured with the tolerance zones set as  $\pm 0.05$  mm. The measuring results of the section ( $Z_4 = 54.34$  mm,  $Z_6 = 87.34$  mm) are shown in Fig. 12.

Figure 12a and b show that the blade grinded with the traditional method can not well meet the required machining accuracy, especially at the LE and TE. The mean error values at  $Z_4 = 54.34$  mm and  $Z_6 = 87.34$  mm were 0.036 mm and 0.023 mm, respectively. The blade edge profiles are rectangular or trapezoidal before grinding due to the previous milling process. The machining accuracy of LE and TE of the traditional method is hard to be controlled as this method lacks the adjustment of the processing parameters according to the machining allowance distribution and MRR model. Therefore, the profiles after grinding remain the same as the profiles before grinding, because this method keeps the machining parameters consistent throughout the machining process. Besides, the setting of processing parameters is heavily dependent on the operator’s operating experience, and over-grinding or under-grinding are prone to occur. Figure 12c and d shows that the blade grinded with the proposed method can be grinded into the tolerance zone well. Figure 13 shows the mean error values of the six sections ( $Z_1 = 22.34$  mm,  $Z_2 = 32.34$  mm,  $Z_3 = 43.34$  mm,  $Z_4 = 54.34$  mm,  $Z_5 = 65.34$  mm,  $Z_6 = 87.34$  mm). The mean error values of the six sections in the proposed toolpath planning method were 0.029 mm, 0.012 mm, 0.022 mm, 0.013 mm, 0.026 mm, and 0.012 mm, which were improved by 63.29%, 66.67%, 67.65%, 43.48%, 29.73%, and  $-8.33\%$  than the traditional method, and the average surface profile accuracy of blades of the proposed methods was 0.019 mm, which was improved by 54.76% than the traditional method. This is because the developed 7th axis can not only be linked with the other 6 axes, but also can precisely control the displacement in the direction of the normal contact force. Combined with the MRR model based on the orthogonal experiment and the proposed toolpath based on the Taylor expansion method, the force-position matching are used to adjust the pressing amount point-by-point on each CC point. Especially at the LE and TE, the allowance distribution is uneven and the difference is large. The point-by-point control of the 7th axis can ensure the accurate material removal, so the profile can be processed closer to the theoretical 3D profile.

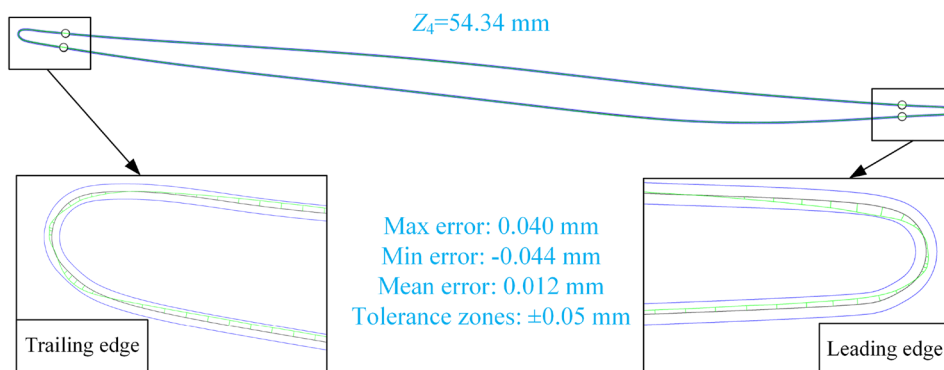
Compared with the traditional toolpath method, the proposed method considers the point-by-point adjustment of the 7th axis for the uneven machining allowance distribution of aero-engine blades. The average surface roughness of the proposed method was 0.34 µm, which was improved by 27.7% than the traditional method. The average profile accuracy error of blades of the proposed methods was 0.019 mm, which was improved by 54.76% than that of the former method. Thus, it fully demonstrates that the improved toolpath method in this paper is better applied to



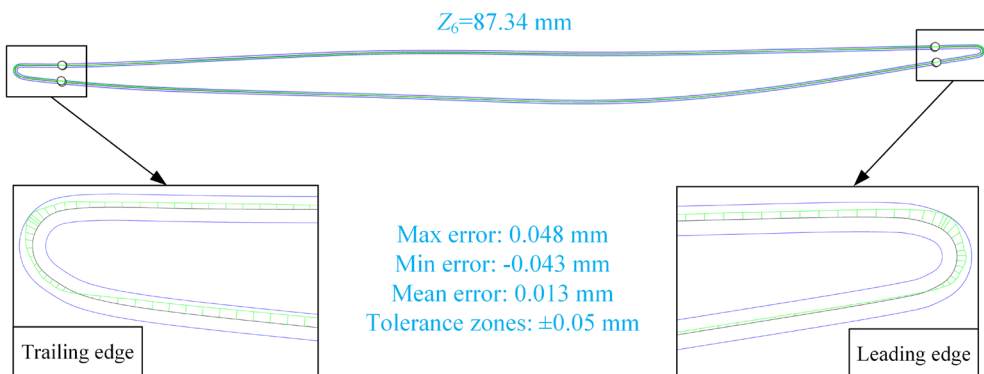
(a)



(b)



(c)



(d)

**Fig. 12** Comparison of blade grinding. **a** Traditional toolpath method ( $Z_4=54.34$  mm). **b** Traditional toolpath method ( $Z_6=87.34$  mm). **c** Proposed toolpath method ( $Z_4=54.34$  mm). **d** Proposed toolpath method ( $Z_6=87.34$  mm)

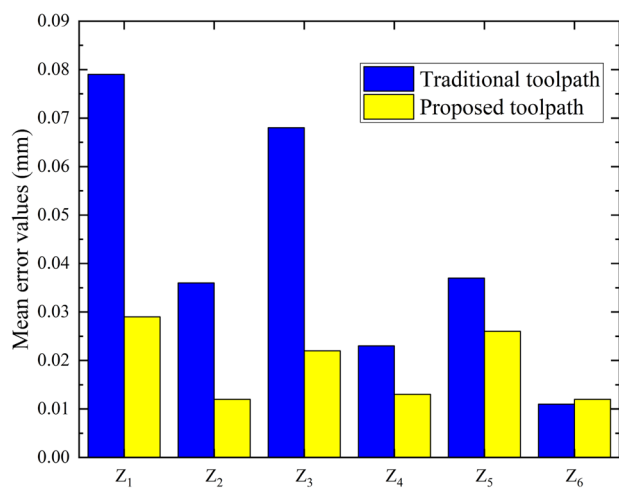


**Fig. 13** Mean error values of six sections

the uneven machining allowance distribution of complex curved surfaces and can meet the requirement of higher profile accuracy.

## 6 Conclusions

In this paper, a novel toolpath planning method for 7-NC grinding of blades is proposed with force-position matching, which comprehensively considers the MRR model, and the point-by-point adjustment of the 7th axis. The proposed method is then verified through comparative experiments on the self-developed machine tool, and the following conclusions are achieved:

1. An MRR model based on force-position matching is established through the orthogonal grinding experiment, and the relationship between the pressing amount and the material removal depth can be effectively predicted. The goodness of fit and correction measurement coefficient are greater than 80%, and the confidence of the regression equation can reach more than 99.98%.
2. The step length of the proposed toolpath method is determined by the equal arc length discretization method and the Taylor formula expansion, avoiding the over-grinding phenomenon caused by the dense CC points at large curvature (especially at the LE and TE). And the post-processing algorithm of CC points is generated based on the double control for the self-developed 7th axis NC machining tool.

3. The average surface roughness and the variation range of surface roughness of the proposed method can reach  $0.34\ \mu\text{m}$  and  $0.14\ \mu\text{m}$ , which were improved by 27.7% and 33.3% than the traditional method. And the average surface profile accuracy of the entire blade can reach  $0.019\ \text{mm}$ , which was improved by 54.76% than that of the former method and falls within the tolerance range of  $\pm 0.05\ \text{mm}$ .

**Acknowledgements** We thank Revealer for their assistance in recording surface images of abrasive belts by high-speed camera 5F01.

**Author contribution** Yilin Mu, Chong Lv and Lai Zou were responsible for planning this paper, Yilin Mu and Heng Li were responsible for experimental work. Yilin Mu, Chong Lv, Heng Li, Lai Zou, Wenxi Wang and Yun Huang were involved in the discussion and significantly contributed to making the final draft of the article. All the authors read and approved the final manuscript.

**Funding** This study was supported by the National Natural Science Foundation of China (Grant No. 52075059) and the Natural Science Foundation of Chongqing (Grant cstc2020jcyj-msxmX0266).

**Availability of data and materials** The authors confirm that the data supporting the findings of this study are available within the article.

## Declarations

**Ethical approval** Not applicable.

**Consent to participate** Not applicable.

**Consent to publish** Not applicable.

**Competing interests** The authors declare no competing interests.

## References

1. Wang T, Zou L, Wan Q, Zhang X, Li Y, Huang Y (2021) A high-precision prediction model of surface roughness in abrasive belt flexible grinding of aero-engine blade. *J Manuf Process* 66:364–375. <https://doi.org/10.1016/j.jmappro.2021.04.002>
2. Wang J, Zhang D, Wu B, Luo M, Zhang Y (2015) Kinematic analysis and feedrate optimization in six-axis NC abrasive belt grinding of blades. *Int J Adv Manuf Technol* 79(1–4):405–414. <https://doi.org/10.1007/s00170-015-6824-9>
3. Zhou K, Liu J, Xiao G, Huang Y, Song K, Xu J, Chen B (2021) Probing residual stress evolution of titanium alloy due to belt grinding based on molecular dynamics method. *J Manuf Process* 66:446–459. <https://doi.org/10.1016/j.jmappro.2021.04.043>
4. Wu S, Kazerounian K, Gan Z, Sun Y (2014) A material removal model for robotic belt grinding process. *Mach Sci Technol* 18(1):15–30. <https://doi.org/10.1080/10910344.2014.863623>
5. Wei H, Peng C, Gao H, Wang X, Wang X (2019) On establishment and validation of a new predictive model for material removal in abrasive flow machining. *Int J Mach Tools Manuf* 138:66–79. <https://doi.org/10.1016/j.ijmactools.2018.12.003>
6. Qi J, Zhang D, Li S, Chen B (2016) A micro-model of the material removal depth for the polishing process. *Int J Adv Manuf Technol* 86(9–12):2759–2770. <https://doi.org/10.1007/s00170-016-8385-y>

7. Ren L, Zhang G, Zhang L, Zhang Z, Huang Y (2019) Modelling and investigation of material removal profile for computer controlled ultra-precision polishing. *Precis Eng* 55:144–153. <https://doi.org/10.1016/j.precisioneng.2018.08.020>
8. Yang Z, Chu Y, Xu X, Huang H, Zhu D, Yan S, Ding H (2021) Prediction and analysis of material removal characteristics for robotic belt grinding based on single spherical abrasive grain model *Int J Mech Sci* 190. <https://doi.org/10.1016/j.ijmecsci.2020.106005>
9. Wang G, Wang Y, Xu Z (2009) Modeling and analysis of the material removal depth for stone polishing. *J Mater Process Technol* 209(5):2453–2463. <https://doi.org/10.1016/j.jmatprotec.2008.05.041>
10. Li J, Wei Z, Wang T, Cheng J, He Q (2017) A theoretical model incorporating both the nano-scale material removal and wafer global uniformity during planarization process. *Thin Solid Films* 636:240–246. <https://doi.org/10.1016/j.tsf.2017.06.020>
11. Fan C, Zhang L, Zhao Q, Zhao J, Zhao J, Sun L (2018) Modeling and optimization of material removal influenced by sliding velocity in polishing. *Proc Inst Mech Eng Part B-J Eng Manuf* 233(4):1127–1135. <https://doi.org/10.1177/0954405418774589>
12. Fan W, Wang W, Wang J, Zhang X, Qian C, Ma T (2020) Microscopic contact pressure and material removal modeling in rail grinding using abrasive belt. *Proc Inst Mech Eng Part B-J Eng Manuf* 235(1–2):3–12. <https://doi.org/10.1177/0954405420932419>
13. Satyarthi MK, Pandey PM (2013) Modeling of material removal rate in electric discharge grinding process. *Int J Mach Tools Manuf* 74:65–73. <https://doi.org/10.1016/j.ijmactools.2013.07.008>
14. Kumar S, Dvivedi A (2020) Development of material removal rate model and performance evaluation of ultrasonic turning process. *Mater Manuf Process* 35(14):1598–1611. <https://doi.org/10.1080/10426914.2020.1784929>
15. Zarepour H, Yeo SH (2012) Predictive modeling of material removal modes in micro ultrasonic machining. *Int J Mach Tools Manuf* 62:13–23. <https://doi.org/10.1016/j.ijmactools.2012.06.005>
16. Bhavsar SN, Aravindan S, Rao PV (2015) Investigating material removal rate and surface roughness using multi-objective optimization for focused ion beam (FIB) micro-milling of cemented carbide. *Proc Inst Mech Eng Part B-J Eng Manuf* 40:131–138. <https://doi.org/10.1016/j.precisioneng.2014.10.014>
17. Fan W, Lee C, Chen J, Xiao Y (2015) Real-time Bezier interpolation satisfying chord error constraint for CNC tool path. *Sci China-Technol Sci* 59(2):203–213. <https://doi.org/10.1007/s11431-015-5949-2>
18. Sarkar S, Dey PP (2015) Tool path planning for machining free-form surfaces. *Trans FAMENA* 39(1):65–78
19. Hu P, Chen L, Tang K (2017) Efficiency-optimal iso-planar tool path generation for five-axis finishing machining of freeform surfaces. *Comput Aided Des* 83:33–50. <https://doi.org/10.1016/j.cad.2016.10.001>
20. Huang Z, Song R, Wan C, Wei P, Wang H (2019) Trajectory planning of abrasive belt grinding for aero-engine blade profile. *Int J Adv Manuf Technol* 102(1–4):605–614. <https://doi.org/10.1007/s00170-018-3187-z>
21. Ma K, Han L, Sun X, Liang C, Zhang S, Shi Y, Wang X (2020) A path planning method of robotic belt grinding for workpieces with complex surfaces. *IEEE-ASME Trans Mechatron* 25(2):728–738. <https://doi.org/10.1109/tmech.2020.2974925>
22. Wen Y, Jaeger DJ, Pagilla PR (2022) Uniform coverage tool path generation for robotic surface finishing of curved surfaces. *IEEE Robot Autom Lett* 7(2):4931–4938. <https://doi.org/10.1109/lra.2022.3152695>
23. Li W, Wang G, Zhang G, Pang C, Yin Z (2016) A novel path generation method of onsite 5-axis surface inspection using the dual-cubic NURBS representation. *Meas Sci Technol* 27(9). <https://doi.org/10.1088/0957-0233/27/9/095003>
24. Wang G, Lv B, Liu B, Mu H (2019) Tool path generation method for three-dimensional vibration-assisted machining. *IEEE International Conference on Mechatronics and Automation*, pp. 1715–1720. <https://doi.org/10.1109/ICMA.2019.8816456>
25. Zhao X, Zhao H, Li X, Ding H (2017) Path smoothing for five-axis machine tools using dual quaternion approximation with dominant points. *Int J Precis Eng Manuf* 18(5):711–720. <https://doi.org/10.1007/s12541-017-0085-5>
26. Sun S, Altintas Y (2021) A G3 continuous tool path smoothing method for 5-axis CNC machining. *CIRP J Manuf Sci Technol* 32:529–549. <https://doi.org/10.1016/j.cirpj.2020.11.002>
27. Yang J, Chen Y, Chen Y, Zhang D (2015) A tool path generation and contour error estimation method for four-axis serial machines. *Mechatronics* 31:78–88. <https://doi.org/10.1016/j.mechatronics.2015.03.001>
28. Chaves-Jacob J, Linares JM, Sprauel JM (2013) Improving tool wear and surface covering in polishing via toolpath optimization. *J Mater Process Technol* 213(10):1661–1668. <https://doi.org/10.1016/j.jmatprotec.2013.04.005>
29. Hatem N, Yusof Y, Kadir AZA, Latif K, Mohammed MA (2021) A novel integrating between tool path optimization using an ACO algorithm and interpreter for open architecture CNC system. *Expert Syst Appl* 178. <https://doi.org/10.1016/j.eswa.2021.114988>
30. Tajima S, Sencer B (2017) Global tool-path smoothing for CNC machine tools with uninterrupted acceleration. *Int J Mach Tools Manuf* 121:81–95. <https://doi.org/10.1016/j.ijmactools.2017.03.002>
31. Huai W, Shi Y, Tang H, Lin X (2019) An adaptive flexible polishing path programming method of the blisk blade using elastic grinding tools. *J Mech Sci Technol* 33(7):3487–3495. <https://doi.org/10.1007/s12206-019-0643-0>
32. Lv C, Zou L, Huang Y, Li H, Wang T, Mu Y (2022) A novel tool-path for robotic adaptive grinding of extremely thin blade edge based on dwell time model. *IEEE-ASME Trans Mechatron* 1–11. <https://doi.org/10.1109/tmech.2022.3156804>

**Publisher's Note** Springer Nature remains neutral with regard to jurisdictional claims in published maps and institutional affiliations.

Springer Nature or its licensor holds exclusive rights to this article under a publishing agreement with the author(s) or other rightsholder(s); author self-archiving of the accepted manuscript version of this article is solely governed by the terms of such publishing agreement and applicable law.